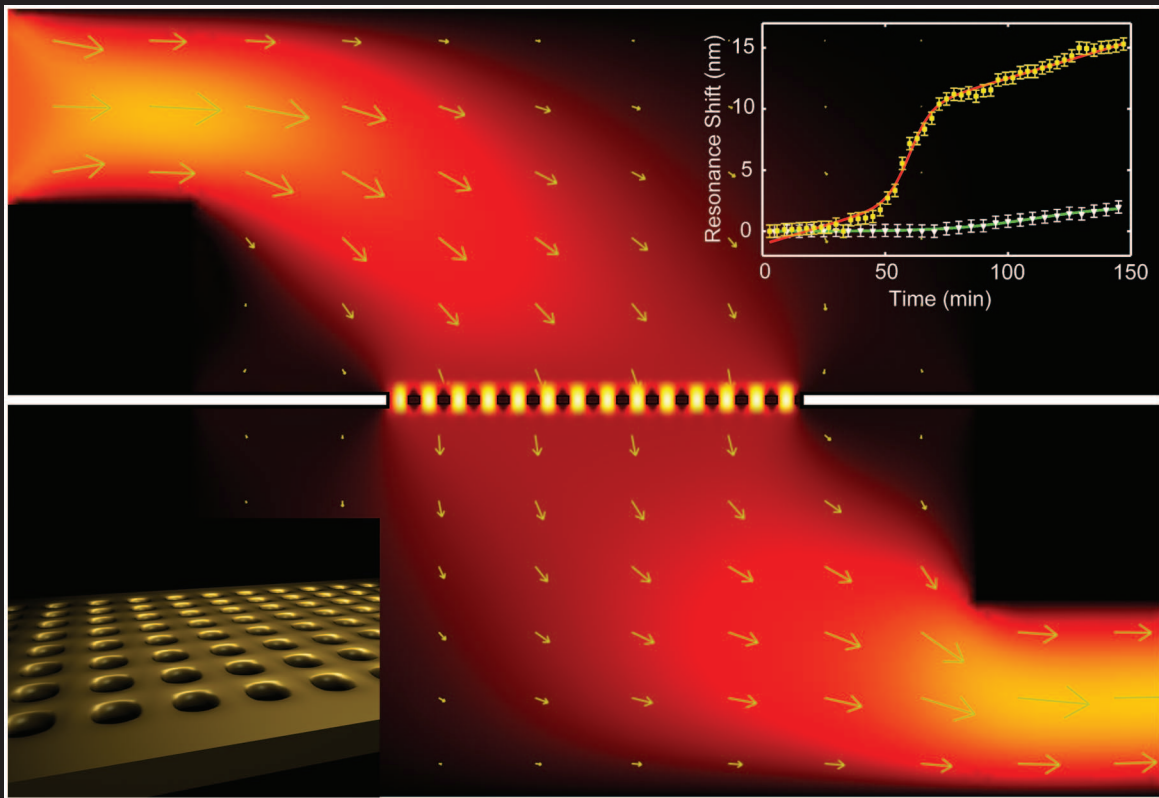


APPLIED PHYSICS LETTERS



0003-6951(20100111)96:2;1-R

AIP

Integrated nanoplasmonic-nanofluidic biosensors with targeted delivery of analytes

Ahmet Ali Yanik,¹ Min Huang,¹ Alp Artar,¹ Tsung-Yao Chang,² and Hatice Altug^{1,a)}

¹Department of Electrical and Computer Engineering and The Photonics Center, Boston University, Boston, Massachusetts 02215, USA

²Department of Electrical Engineering, Massachusetts Institute of Technology, Cambridge, Massachusetts 02139, USA

(Received 1 October 2009; accepted 19 November 2009; published online 11 January 2010)

Performances of the biosensors are often limited by the depletion zones created around the sensing area which impede the effective analyte transport. To overcome this limitation, we propose and demonstrate a nanoplasmonic-nanofluidic sensor enabling targeted delivery of analytes to the sensor surface with dramatic improvements in mass transport efficiency. Our sensing platform is based on extraordinary light transmission effect in suspended plasmonic nanoholes. This scheme allows three-dimensional control of the fluidic flow by connecting separate layers of microfluidic channels through plasmonic/nanofluidic holes. To implement the proposed sensor platform, we also introduce a lift-off free nanofabrication method. © 2010 American Institute of Physics.

[doi:10.1063/1.3290633]

Label free biosensors, offering a rapid way to obtain equilibrium and rate constants of the biomolecular interaction, have taken much interest recently.¹ In particular, nanoscale optical biosensors with high multiplexing capabilities and signal to noise ratios are promising for detection of low concentrations of analytes.^{2,3} However, performances of surface biosensors are often limited in a fluidic environment by the inefficient analyte (mass) transport instead of their intrinsic detection capabilities.^{4,5} As the analytes are collected by the functionalized surface, a depletion zone forms around the sensing area where the analyte transport is diffusive.⁴ Depletion zone expands with time until the convective flow ceases its further growth. Randomized nature of the mass transport in the depletion zone severely limits the delivery of the analytes from the convective flow to the sensor surface. At low concentrations, this limitation causes impractically long detection times.⁵ One can compress the extent of these depletion zones by increasing the convective flow rate.⁵ However, such a passive control scheme often results in moderate improvements of the device performances due to the shorter times required for analytes to stream pass the sensing surface. Stirring of the depletion zone using various mixing strategies also seem to result in moderate enhancements in performances.^{6,7} Innovative approaches are needed to overcome the mass transport limitations. One of the main conceptual constraints in previous approaches is that microfluidics and biosensing are always considered as different parts of a sensor platform completing each other but not a fully merged single entity.

In this article, we propose and demonstrate a hybrid biosensing system merging nanoplasmonics and nanofluidics in a single platform. Unlike convectional approaches where the analytes simply stream pass over the surface, our platform enables targeted delivery of the analytes. Using our platform, we show 14-fold improvement in the mass transport rate constants. Considering that this rate constant appears in the exponential term, such an improvement means superior ana-

lyte delivery to the biosensor surface at low concentrations. Our detection platform is based on extraordinary light transmission effect (EOT) in suspended plasmonic nanohole arrays.⁸ The nanoholes here act as nanofluidic channels connecting the fluidic chambers on both sides of the sensors. To fabricate these nanostructures, we introduce a lift-off free plasmonic device fabrication technique based on positive resist electron beam lithography. The simplicity of this fabrication technique allows us to fabricate nanostructures with extremely high yield/reproducibility and minimal surface roughness. As a result, we achieve higher refractive index sensitivities ($\Delta\lambda/\Delta n=630$ nm/RIU) with respect to the previous studies based on simple nanohole arrays.^{9,10} We believe this fabrication technique can find wide range of applications in nanoplasmonics field by eliminating the need for operationally slow and expensive focused ion beam lithography. A unique property of our sensing platform is that it also offers an extra degree of freedom in microfluidic circuit engineering by connecting separate layers of microfluidic circuits through biosensors. Through this platform, it is possible to create “multilayered lab-on-chip systems” allowing three dimensional control of the fluidic flow.

Lift-off free fabrication scheme, we introduce here, is summarized in Figs. 1(a) and 1(b). It is based on single layer e-beam lithography and reactive ion etching (RIE). Fabrication process starts with a silicon wafer with low pressure chemical vapor deposition silicon nitride (SiN_x) films on both sides. By optical lithography and dry/wet etching methods, we form free standing SiN_x membranes (50 nm thick). These membranes are later coated with positive e-beam resist poly(methyl methacrylate) and then e-beam lithography is performed. Nanohole pattern (with hole diameters of 220 nm and a periodicity of 600 nm) is transferred to the suspended SiN_x film through a dry etching process [Fig. 1(a)]. E-beam resist is later removed with an oxygen plasma cleaning process leaving only a patterned SiN_x film with air on both sides [Fig. 1(c)]. Finally, we use a directional e-beam evaporator to deposit Ti (5 nm) and Au (125 nm) metal layers defining the suspended plasmonic sensors with nanohole openings [Fig.

^{a)}Electronic mail: altug@bu.edu.

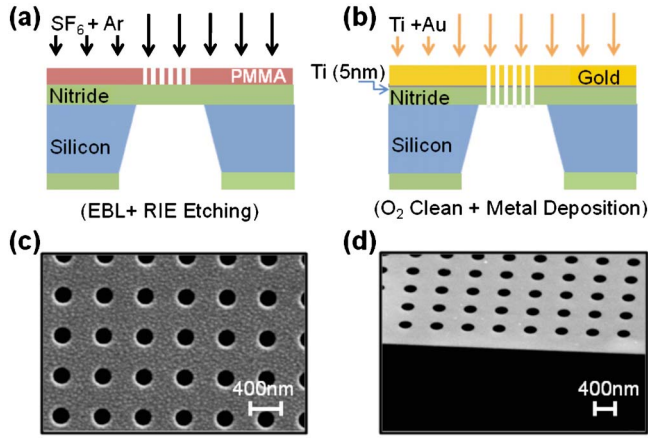


FIG. 1. (Color online) Suspended plasmonic nanohole arrays are fabricated using a single layer lithography process consisting of following steps: (a) e-beam lithography and pattern transfer with RIE etching, (b) surface cleaning with oxygen plasma and metal deposition. [(c) and (d)] Scanning electron images of the nanoholes are shown from different angles for nanohole arrays with 200 nm in diameter and 600 nm in periodicity.

1(b)]. This deposition process is observed to be extremely reliable; large areas of metallic nanohole arrays are repeatedly obtained without clogging the openings. Only a small shrinking in nanohole diameter ($<4\%$) is observed after gold deposition due to a slight coverage of the nanohole sidewalls [Figs. 1(c) and 1(d)].

Fabricated arrays are mounted in a custom designed multilayered microfluidic channel system based on poly-(dimethylsiloxane). As illustrated in Figs. 2(a) and 2(b), this multi-inlet/outlet fluidic platform allows us to actively control the fluidic flow in three dimensions through the plasmonic nanohole openings. Convective flow over different surfaces of the plasmonic sensor is realized by running the solutions in between input \rightarrow output lines on the same side, such as $1 \rightarrow 2/3 \rightarrow 4$ [Fig. 2(a)]. In this arrangement, mixing of liquid flowing above the gold surface and below the SiN_x membrane is minimal (diffusive) and the convective flow in separate channels is nearly independent. In actively controlled (targeted) delivery scheme, the convective flow is steered perpendicularly toward the plasmonic sensing surface by allowing the flow only through one inlet/outlet on either side of the plasmonic sensor [Fig. 2(b)]. Flow could be directed from top-to-down and down-to-top directions by enabling flow between $1 \rightarrow 4$ and $3 \rightarrow 2$, respectively.

Targeted delivery of the analytes to the sensing surface is demonstrated in spectral measurements as shown in Fig. 3(a). Initially, both the top and the bottom channels are filled

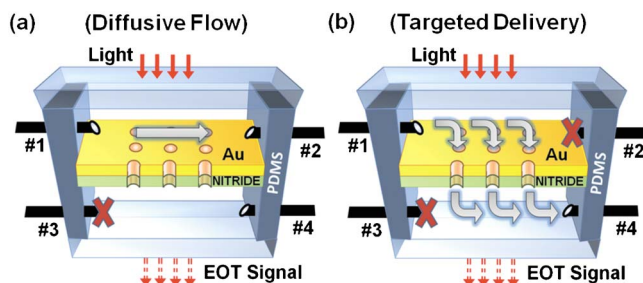


FIG. 2. (Color online) Multilayered microfluidic scheme allows three-dimensional control of the convective flow enabling (a) passive (diffusive) and (b) active (targeted delivery) transport of the analytes to the sensing surface. Perpendicular steering of the convective flow is achieved by allowing flow only through one of the inlet/outlets of the top/bottom channels (b).

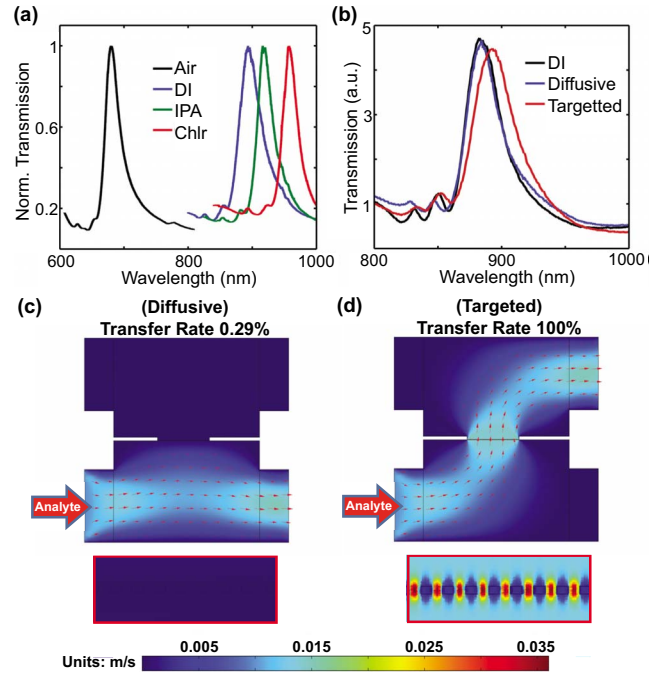


FIG. 3. (Color online) (a) Bulk refractive index sensitivity of the plasmonic nanohole arrays are obtained in different solutions. (b) Resonance shifts for the passively and actively controlled mass transport schemes are compared after running IPA (analyte) for 10 min at $20 \mu\text{m}/\text{min}$ flow rate. Microfluidic simulations demonstrate (c) low transfer rates for the passive transport scheme due to the weaker perpendicular flow of the analytes, while (d) much more efficient mass transport toward the surface is observed for the targeted delivery scheme.

with a low refractive index liquid, deionized (DI) water ($n_{\text{DI}}=1.333$), at a high flow rate ($550 \mu\text{L}/\text{min}$). Once the channels are filled with DI water completely, the plasmonic resonance shifts from $\lambda_{\text{air}}=679 \text{ nm}$ (air on both sides) to $\lambda_{\text{DI}}=889 \text{ nm}$ (DI on both sides). This corresponds to a bulk refractive index sensitivity of $\Delta\lambda/\Delta n=630 \text{ nm}/\text{RIU}$, which is also confirmed in independent measurements [Fig. 3(a)] performed in acetone ($n_{\text{acetone}}=1.356$), IPA ($n_{\text{IPA}}=1.377$) and chloroform ($n_{\text{chloroform}}=1.49$). As plasmons at the Ti/SiN interface are suppressed by the losses, this shift only reflects the spectral response of the EOT resonance to the changing refractive index in the top channel. The spectrum, obtained once the channels are filled with DI-water, is used as a background for the following measurements. To quantify the analyte transport efficiency of the both delivery schemes, a lower viscosity analyte solution (IPA) with higher refractive index is introduced from the bottom inlet. The plasmonic sensor responds only to the refractive index change due to the perpendicularly diffused or actively delivered IPA solution depending on the implemented flow scheme. This way, a good quantitative measure of the transport limit is created in perfect collection case.⁴ In the diffusive transport scheme, IPA solution is pumped into the bottom channel ($20 \mu\text{L}/\text{min}$) and collected from the bottom side while the top outlet is kept open. A relatively small red shifting of the plasmonic resonance $\Delta\lambda=\lambda_{\text{IPA}}^{10 \text{ min}}-\lambda_{\text{DI}}=1.2 \text{ nm}$ [blue curve in Fig. 3(b)] from DI-water background [black curve in Fig. 3(b)] is recorded after running the IPA solution for 10 min. We attribute the minute resonance shift to the limited delivery of the IPA to the sensing surface. Although the flow through the top outlet is also allowed, this shows that perpendicular flow of the IPA is very weak. This observation is

also confirmed with microfluidics simulations as discussed below [Fig. 3(c)]. For targeted delivery of the convective current to the surface, IPA is directed from down-to-top direction by enabling flow between 3 \rightarrow 2. In this case, a much larger red shifting ($\Delta\lambda=10$ nm) of the plasmonic resonance from DI-water background is obtained after flowing IPA solution for 10 min at the same flow rate (20 $\mu\text{L}/\text{min}$). This clearly shows that the targeted delivery scheme created in our nanoplasmonic-nanofluidic platform allows more efficient analyte transport to the sensor surface and improves the sensor performance.

Microfluidics simulations are performed to confirm the experimental conclusions. Scaled down version of the microfluidic system is simulated using a finite elements method using COMSOLTM software. Calculations are done in two-dimensions using incompressible Navier–Stokes equations. Boundaries of the simulation domain are defined as 200 μm in height and 500 μm in width for each of the channels with 150 μm inlet openings. We employ a refined mesh near the sensor area where the flow rate is high and turbulences occur. Figures 3(c) and 3(d) shows the steady state solutions of the velocity field profile of the fluidic flow. Transfer rate, reflecting the ratio of the perpendicular flow to the inlet flow, is used to quantify the performance of the delivery scheme. In accordance with our experimental observations [Fig. 3(b)], when IPA solution is injected and collected from the bottom channel, a very weak perpendicular flow of the IPA solution toward the top channel is observed [Fig. 3(c)]. Although liquid flow through the top outlet is allowed in the simulations, the flow rate at this outlet is calculated to be extremely small (only 0.29% of the input flow). On the other hand, active directing of the convective stream toward the surface and through the nanoholes (inset) results in a transfer flow rate of 100% [Fig. 3(d)]. Accordingly, in an arrangement where the fluidics is flowed in and out from different sides of the biosensor, all the fluidic current is actively transferred through the nanohole openings. Simulations also indicate that flow through the nanofluidic channels creates turbulences and stirring of the solution as it passes through the device (not shown). This stirring process is expected to further improve the mass transport rate.

Time dependent spectral measurements are performed to characterize the efficiency of the analyte delivery to the sensing surface for both schemes (at a flow rate of 4 $\mu\text{L}/\text{min}$). As shown in Fig. 4, the directed delivery results in a larger resonance shift compared to the passive one, indicating a much more efficient mass transport to the biosensor area. Experimentally observed resonance shifts are (least-squares) fitted to a sigmoid function of form $A_b + (A_t - A_b)/(1 + e^{-k(t-t_0)})$.¹¹ This is superposed to a linearly increasing background with $C_t(t-t_0) + C_0$ due to increasing refractive index of the bulk medium in the top channels as IPA concentration increases. The mass transport rate constants are obtained as $k_{\text{pass}}=0.0158$ min^{-1} and $k_{\text{act}}=0.2193$ min^{-1} for the passive and targeted transport schemes, respectively. This corresponds to more than 14-fold improvement in rate constants which is crucial for enhancing the performance in immunoassay based applications.⁵ After more than 10 h of operation at compatible flow rates for biosensing applications (4 $\mu\text{L}/\text{min}$), we observed that the membranes and the plasmonic devices are intact. Similarly, no structural deforma-

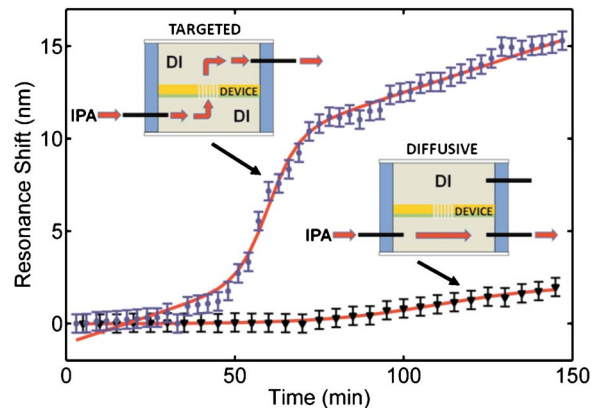


FIG. 4. (Color online) Efficiencies of the passive (triangles) and targeted (squares) delivery of the analytes are compared in real time measurements. 14-fold improvement in mass transport rate constant is observed for the targeted delivery scheme.

tions are observed in the spectral measurements showing the reliability of the devices.

In conclusion, we have proposed and demonstrated a hybrid biosensing system merging nanoplasmonics and nanofluidics in a single platform with targeted delivery of analytes to the sensor surface. To realize our proposal, we developed a lift-off free nanofabrication scheme allowing us to manufacture plasmonic nanohole biosensors with ease and high reliability/uniformity. High sensitivities ($\Delta\lambda/\Delta n=630$ nm/RIU) to the refractive index changes are obtained confirming the quality of the fabricated nanostructures. In order to control the convective transport in three dimensions, we introduced a multilayered microfluidics scheme enabling an extra degree of freedom in fluidic/sensor design. We demonstrated 14-fold improvement in the mass transport rate constants. Such improvements in the exponential term reflect the superior mass transport capability of the targeted delivery scheme demonstrated here. These hybrid biosensors can find wide range of applications in point-of-care applications as well as research studies on drug development and protein-protein interactions.

This work is supported in part by NSF SGER Award (Award No. ECSS-0849603), Massachusetts Life Science Center New Investigator Award (H.A.), Boston University Photonics Center, and NSF Engineering Research Center on Smart Lighting (Grant No. EEC-0812056).

- ¹S. Srivastava and J. LaBaer, *Nat. Biotechnol.* **26**, 1244 (2008).
- ²J. N. Anker, W. P. Hall, O. Lyandres, N. C. Shah, J. Zhao, and R. P. Van Duyne, *Nature Mater.* **7**, 442 (2008).
- ³A. Artar, A. A. Yanik, and H. Altug, *Appl. Phys. Lett.* **95**, 051105 (2009).
- ⁴P. E. Sheehan and L. J. Whitman, *Nano Lett.* **5**, 803 (2005).
- ⁵T. M. Squires, R. J. Messinger, and S. R. Manalis, *Nat. Biotechnol.* **26**, 417 (2008).
- ⁶S. K. Yoon, G. W. Fichtl, and P. J. A. Kenis, *Lab Chip* **6**, 1516 (2006).
- ⁷R. A. Vijayendran, K. M. Motsegood, D. J. Beebe, and D. E. Leckband, *Langmuir* **19**, 1824 (2003).
- ⁸A. A. Yanik, X. Wang, S. Erramilli, M. K. Hong, and H. Altug, *Appl. Phys. Lett.* **93**, 081104 (2008).
- ⁹A. G. Brolo, R. Gordon, B. Leathem, and K. L. Kavanagh, *Langmuir* **20**, 4813 (2004).
- ¹⁰A. De Leebeek, L. K. S. Kumar, V. De Lange, D. Sinton, R. Gordon, and A. G. Brolo, *Anal. Chem.* **79**, 4094 (2007).
- ¹¹C. García-Aljaro, X. Muñoz-Berbel, A. T. A. Jenkins, A. R. Blanch, and F. X. Muñoz, *Appl. Environ. Microbiol.* **74**, 4054 (2008).